MDPI

Article

Fault Detection of Bearing by Resnet Classifier with Model-Based Data Augmentation

Lu Qian [1], Qing Pan [2], Yaqiong Lv [1] and Xingwei Zhao [3,*]

1   School of Transportation and Logistics Engineering, Wuhan University of Technology, Wuhan 430070, China; qianlu@whut.edu.cn (L.Q.); y.q.lv@whut.edu.cn (Y.L.)
2   State Key Laboratory of High Performance Complex Manufacturing,
     School of Mechanical and Electrical Engineering, Central South University, Changsha 410083, China;
     panqing0905@csu.edu.cn
3   State Key Laboratory of Digital Manufacturing Equipment and Technology,
     Huazhong University of Science and Technology, Wuhan 430074, China
*   Correspondence: zhaoxingwei@hust.edu.cn

Abstract: It is always an important and challenging issue to achieve an effective fault diagnosis in rotating machinery in industries. In recent years, deep learning proved to be a high-accuracy and reliable method for data-based fault detection. However, the training of deep learning algorithms requires a large number of real data, which is generally expensive and time-consuming. To cope with this, we proposed a Resnet classifier with model-based data augmentation, which is applied for bearing fault detection. To this end, a dynamic model was first established to describe the bearing system by adjusting model parameters, such as speed, load, fault size, and the different fault types. Large amounts of data under various operation conditions can then be generated. The training dataset was constructed by the simulated data, which was then applied to train the Resnet classifier. In addition, in order to reduce the gap between the simulation data and the real data, the envelop signals were used instead of the original signals in the training process. Finally, the effectiveness of the proposed method was demonstrated by the real bearing experimental data. It is remarkable that the application of the proposed method can be further extended to other mechatronic systems with a deterministic dynamic model.

Keywords: bearing fault detection; deep residual network; data augmentation

1. Introduction

As an indispensable element of rotating machinery, the rolling bearing plays an effective and crucial role in real industries, whose operation status profoundly influences the performance of rotating machinery equipment. If faults occur in critical bearings, it may cause costly downtime and catastrophic accidents. Therefore, having an effective and accurate fault diagnosis of bearings is critical to improving the reliability and safety of rotating machinery equipment.

During the past decades, the fault detection and diagnosis of roller bearings have been receiving increasing attention and have been a research hotspot. Due to the distinctive characteristics of the vibration signals produced by a faulty bearing, such as its periodicity and sensitivity to faults, great efforts have been made to develop a bearing fault diagnosis based on vibration-based methods. Model-based methods are devoted to revealing the fault generation mechanism and finding the fault-related information according to the map from inputs to responses [1,2]. Meanwhile, a few model-based methods have also been applied for degradation data analysis and the remaining useful life estimation and prediction [3,4]. In addition, numerous signal processing methods have been used to reduce the noise and extract and highlight the fault-related features in vibration signals to achieve an accurate fault diagnosis [5,6]. These methods can be classed into three categories on the basis of the

fundamentals of signal processing methods. The first is time-domain analysis [7], such as the peak value, standard deviation and kurtosis, and so on. Frequency domain analysis, typified by fast Fourier frequency transform (FFT) [8], is the second category. The third kind is time-frequency domain analysis, including short-time Fourier transform (STFT) [9], wavelet transform [10,11] and empirical mode decomposition (EMD) [12], and so forth. However, most of the available traditional signal-based methods presently require human intervention and sufficient expert knowledge on the diagnosis of an object and signal processing, which limits their industrial application to mechanical equipment fault diagnosis. In this regard, alternative methods should be developed for a bearing fault diagnosis.

To overcome the limitations of demands of prior expertise based on the signal-based methods and achieve higher performance, machine learning techniques have already been widely applied in mechanical fault diagnoses [13]. Based on the machine learning techniques, fault diagnosis is regarded as a classification problem. In the traditional machine learning methods, representative features are first extracted from the raw signals, based on which pattern of recognition technology is applied to classify the health conditions of the equipment, for instance, support vector machines (SVM) [14], clustering algorithms [15] and artificial neural networks (ANN) [16,17] and so on. Shi et al. [18] applied linear discriminant analysis and gray wolf optimizer to improve the SVM algorithm and enhance the performance of fault classification. Zhang et al. [19] applied the BP neural network algorithm, which was based on the transfer component analysis, to detect the bearing fault states. In spite of the success achieved by these methods of fault diagnosis in the past years, it is still a challenge to ensure fault diagnosis accuracy with highly complex nonlinear signals. Due to the high performance in dealing with nonstationary signals, the deep learning method has recently been developed for feature extraction and pattern recognition [20]. Lei et al. [21] presented a framework for intelligent fault diagnosis, where a two-layer neural network with sparse filtering was constructed to learn the features from raw mechanical signals directly. Additionally, based on these learned features, the mechanical faults were identified by the classifier. Kolar et al. [22] propose a multi-channel deep convolutional neural network configuration for a rotary-machinery state classification. Janssens et al. [23] proposed a feature learning model for the bearings condition monitoring, based on convolutional neural networks, which removed the need for expert knowledge related to feature extraction compared with the classical statistical feature analysis. Mao et al. [24] proposed a multiple-fault diagnosis method that was based on deep output kernel learning, in which the depth features were extracted adaptively by an auto encoder neural network and thus, by means of solving the objective function constructed by the output kernel regularizer, the fault classifier was constructed. Due to the powerful capacity for classification and excellent convergence behaviors, deep learning methods can learn the deep features of different data and distinguish them automatically. However, deep learning methods require a large number of datasets to achieve a high accuracy of classification [25]. The industrial applications are limited by the requirement of in-service data under a wide range of operating conditions, which is generally an expensive and time-consuming practice to carry out dozens of experiments, especially for the key components in large machinery and equipment.

To deal with this issue, researchers have started to focus on the data augmentation method to extend the amount of available data with limited in-service data. Data augmentation is first applied in the field of two-dimensional images, and then the available images are transformed into new images by various means [26,27]. To solve the problem of the paucity of data, some approaches were developed based on data augmentation to deal with one-dimensional signals. To achieve the engineering prognostics, Kim et al. [28] proposed a run-to-fail (RTF) data augmentation method based on the dynamic time warping (DTW) technique, where a neural network was trained for the remaining useful life prediction of the current system by using the other system's RTF data. A semi-supervised learning (SSL) approach, based on data augmentation and metric learning, was proposed by Yu et al. [29]. Seven data augmentation strategies were applied to expand the feature space with limited

labeled data. However, the data augmentation was realized by transforming the available signals into new signals in these studies, which led to limited distribution and feature space of the dataset. To overcome this barrier, simulation-driven machine learning methods were studied to create the training data, including a variety of operating conditions, which can be combined with available in-service fault data for the fault diagnosis. A data simulation by resampling (DSR) method was proposed by Hu et al. [30] to generate various working conditions of data for fault diagnoses. Lu et al. [31] proposed a vibration-based classification approach using model-based data augmentation for light-weight robotic-drilling-condition identification, where a dynamic model for a robotic drilling system was built to generate signals for the training data augmentation. Sobie et al. [32] generated training data by using information gained from high-resolution roller bearing dynamics simulations. Then, the machine learning algorithms were trained with the simulated data to classify the bearing faults. However, the roller bearing dynamics in this study are considered as a linear system, in which the race defect is modeled with a prescribed force, and the interaction between each element caused by faults is neglected. There exist certain differences with the actual situation.

Motivated by the aforementioned studies, we developed a fault detection approach based on data augmentation for roller bearing in this paper, which integrated a model-based method and deep learning method. To be specific, a dynamic model of a roller bearing was first established to reflect the correspondence between the bearing states and vibration signals. Then, the data augmentation was achieved by the simulated signals generated by the dynamic model, and based on this, a fault classifier was trained by a deep learning algorithm. Moreover, the envelop signals were used instead of the original signals in the training process to reduce the gap between the simulated data and the real data. Finally, the operation states of the roller bearings could be identified by the trained fault classifier by inputting the vibration signals to be classified.

The remainder of the paper is organized as follows: Section 2 introduces the framework of the proposed method in detail, including the model-based data augmentation and deep residual network classification. The experimental study will be presented and discussed in Section 3. Finally, some conclusions are given in Section 4.

2. Methodology of Data Augmentation

Model-based methods and data-driven methods have demonstrated the effectiveness and performance of fault diagnosis of machines [1,33,34]. Model-based methods show advantages in providing the map from inputs to responses and revealing the fault generation mechanism. However, it is less effective in dealing with data at a low signal-to-noise ratio (SNR). By contrast, intelligent fault diagnosis methods can achieve reliable diagnostic results with complex signals. However, massive datasets are required to ensure classification accuracy, which brings about a high cost of data collection and training. To detect the bearing state with less real data, a fault detection method for bearings based on data augmentation is proposed in this paper, which integrates the model-based methods and data-driven methods. To this end, based on the physics knowledge and failure mechanism of the bearings, a dynamic model was constructed to generate the vibration signals of the bearing to alleviate the problem of data acquisition. Then, the generated dataset was used to realize the data augmentation, and the deep learning algorithm was applied to train the fault classifier. Moreover, the envelop signals were used instead of the raw signals in the training process to reduce the gap between the simulated data and the real data. Finally, a reliable fault classifier insensitive to noise signals was obtained. The operation states of the rolling bearings can be delivered by the fault classifier by inputting the vibration signals to be classified. The framework of the proposed method is shown in Figure 1.
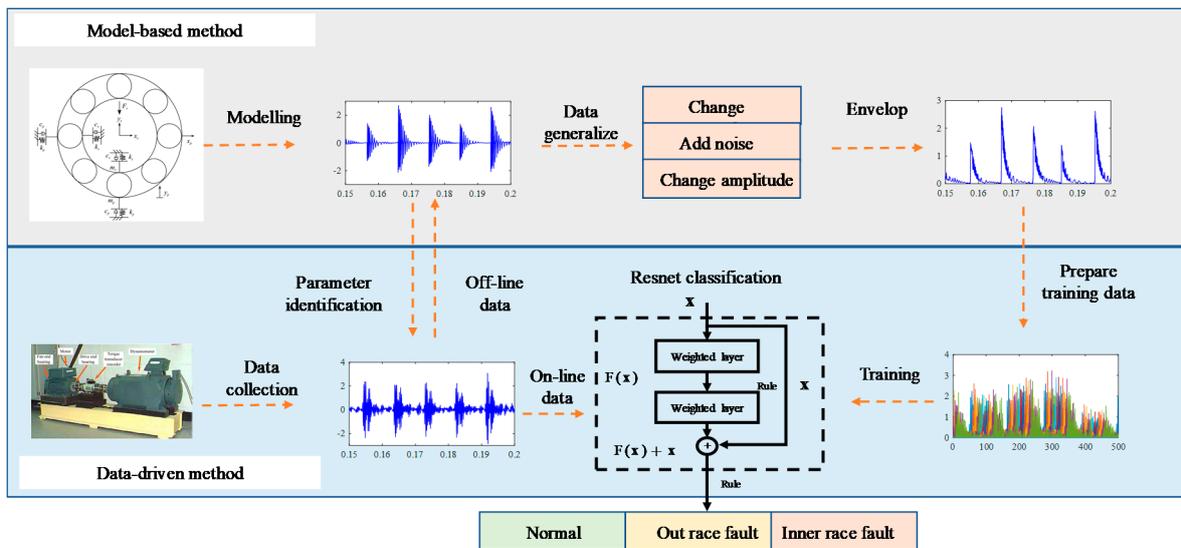
Figure 1. Framework of the fault detection by Resnet classifier with model-based data augmentation.

2.1. Model-Based Data Augmentation

To analyze the structural vibration characteristics of the rolling element bearing, the contact between the outer race and other components can be considered as a spring-mass system, in which the outer race is fixed on a pedestal, and the inner race is fixed with the shaft. The sensor is placed on the pedestal with an outer race to detect high-frequency natural vibrations of the bearing. Thus, to provide the vibration response signals of the rolling bearings containing different working states, a vibration model with four degrees of freedom (DOFs) was constructed by considering the movements in the horizontal and vertical directions of the inner race and outer race, as shown in Figure 2.
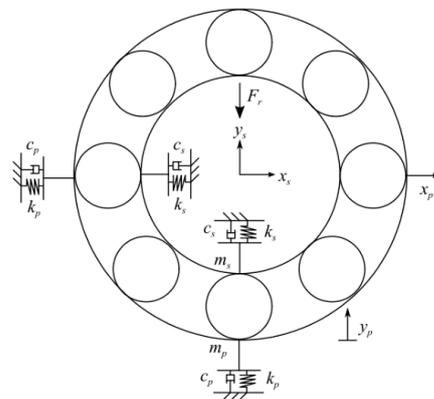

Figure 2. Vibration model of rolling element bearing.

Considering the vibration of the outer race and inner race in a vertical direction, the dynamic equation of the bearing system can be described as:

$$
\begin{aligned}
m_s\ddot{x}_s + c_s\dot{x}_s + k_s x_s + F_x &= 0 \\
m_s\ddot{y}_s + c_s\dot{y}_s + k_s y_s + F_y &= F_r \\
m_p\ddot{x}_p + c_p\dot{x}_p + k_p x_p &= F_x \\
m_p\ddot{y}_p + c_p\dot{y}_p + k_p y_p &= F_y
\end{aligned}
\tag{1}
$$

where x_s and x_p denote the displacement of the inner race and outer race in the x direction, y_s and y_p represent the displacement of two raceways in the y direction, accordingly. F_x and F_y are the elastic contact force between the raceways and the rolling elements in the x

and y direction, and F_r is the radial load generally produced by the weight of the shaft and the rotor. Other parameters in Equation (1) can refer to the given nomenclature table.

According to the Hertz contact theory, the contact force between the raceways and the rolling elements can be given as

$$f = k_b \delta^n \tag{2}$$

where k_b represents the load-deflection factor which depends on the contact geometry and the elastic contacts of the material. δ is the overall contact deformation of the rolling elements, which is composed of the contact deformation of each rolling element. The exponent $n = 1.5$ for ball bearings and $n = 1.1$ for roller bearings.

When the bearings operate, part of the raceway will be in the load zone, and the other part of the raceway will be in the non-load zone, which is shown in Figure 3. The contact deformation of each rolling element is determined by the angular position of the rolling element, the relative displacement between the inner and outer races, and the bearing clearance. The calculation of the contact deformation of the jth rolling element can be given as

$$\delta_j = (x_s - x_p)\cos\phi_j + (y_s - y_p)\sin\phi_j - c, j = 1, 2, \ldots, n_b \tag{3}$$

where n_b denotes the number of the rolling elements. According to the elasto-hydrodynamic lubrication (EHL) theory, the clearance value c is set as negative, owing to the effect of oil EHL film [28]. The angular positions of the jth rolling element ϕ_j can be described as

$$\phi_j = \frac{2\pi(j-1)}{n_b} + \omega_c dt + \phi_0$$
$$\omega_c = (1 - \frac{D_b}{D_p})\frac{\omega_s}{2} \tag{4}$$

where ω_c is the angular velocity of the bearing cage, ϕ_0 denotes the initial angular position of the bearing cage, D_b is ball diameter and D_p is the pitch circle diameter of the bearing, ω_s is the angular velocity of the shaft.
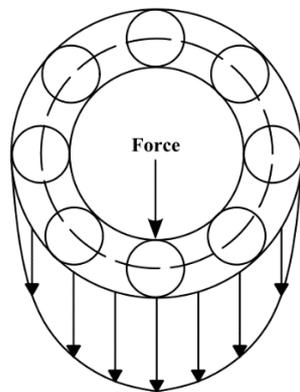

Figure 3. Load distribution of roller bearing.

According to Equations (2) and (3), summing up the contact forces of the n_b rolling elements, the overall nonlinear elastic contact forces of the bearing in the x and y directions can be calculated as

$$F_x = k_b \sum_{j=1}^{n_b} \gamma_j ((x_s - x_p)\cos\phi_j + (y_s - y_p)\sin\phi_j - c)^{1.5} \cos\phi_j$$
$$F_y = k_b \sum_{j=1}^{n_b} \gamma_j ((x_s - x_p)\cos\phi_j + (y_s - y_p)\sin\phi_j - c)^{1.5} \sin phi_j \tag{5}$$

where γ_j is a switch function which depends on the positive and negative values of the contact deformation δ_j, described as

$$\gamma_j = \begin{cases} 1 \ if \ \delta_j > 0 \\ 0 \ otherwise \end{cases} \tag{6}$$

It is noticed that the vibration model of the bearings presented above does not take different fault types into consideration. To simulate the vibration of the localized faults on the different components of bearings, the effects of the localized faults will be considered in the vibration model. The dynamic equation of the bearing system with faults can still be given by Equation (1). The main difference lies in the expression of the contact deformation of the rolling elements.

If a bearing operates in the health state at a steady speed, all forces in the bearing are in quasi-equilibrium. Once a localized fault occurs in the inner and outer races or the rolling elements, a certain deformation will be suddenly released when the fault contacts other components. As a result, a rapid change will take place in the elastic deformation of the components, and the force equilibrium state will be disturbed. Considering the new variations in the model with localized faults, the contact deformation of the jth rolling element is rewritten as

$$\delta_j = (x_s - x_p)\cos\phi_j + (y_s - y_p)\sin\phi_j - c - \overbrace{\beta_j c_d}^{\text{fault part}} \tag{7}$$

where c_d denotes the fault depth. β_j is a switch function to describe whether there is a contact loss due to the fault depth, which is closely related to the angular position of the faults. In addition, different fault types bring about different expressions of switch functions β_j. In what follows, the expressions of the switch functions for the different localized faults will be discussed in terms of the outer race fault, inner race fault, and the fault in the rolling elements.

a. Outer race fault

When the outer race exists as the local fault, such as a spall, the switch function β_j is expressed as

$$\beta_j = \begin{cases} 1 & \text{if } \phi_d < \phi_j < \phi_d + \Delta\phi_d \\ 0 & \text{otherwise} \end{cases} \tag{8}$$

In this case, the spall is fixed in the outer race located from the defined angular position ϕ_d to $\phi_j + \Delta\phi$. Here, phi_d is a constant value, and $\Delta\phi$ is related to the fault length.

b. Inner race fault

In the case of the inner race fault, the local fault rotates with the inner race and the shaft. The switch function β_j is given as

$$\beta_j = \begin{cases} 1 & \text{if } \omega_s t + \phi_{d0} < \phi_j < \omega_s t + \phi_{d0} + \Delta\phi_d \\ 0 & \text{otherwise} \end{cases} \tag{9}$$

In this case, the angular position of the fault ϕ_d will change with the speed of the shaft. Here, $\phi_d = \omega_s t + \phi_{d0}$, where ω_s denotes the angular velocity of the shaft and ϕ_{d0} is the initial angular position of the fault.

c. Fault in rolling elements

It is more complicated when a local fault occurs in a rolling element. The fault will rotate with the rolling element. The angular position of the fault is described as

$$\phi_s = \omega_r t + \phi_{d0}$$
$$\omega_r = \frac{\omega_s}{2}\frac{D_p}{D_b}\left(1 - \left(\frac{D_p}{D_b}\cos\alpha\right)^2\right) \tag{10}$$

where ω_r is the angular velocity of the rolling element, and α is the contact angle.

When there exists a fault in the rolling element *k*, the fault will make contact with both the inner and outer races. The switch values and the fault periods will differ for both races due to the difference in the raceway curvature between the inner and outer races. Therefore, the switch function β_j is defined as

$$\beta_j = \begin{cases} 0, j \neq k \\ 1, \text{ if } 0 < \phi_s < \Delta\phi_{do}, j = k \\ \frac{c_{dr}+c_{di}}{c_{dr}-c_{do}}, \text{if } \pi < \phi_s < \pi + \Delta\phi_{di}, j = k \\ 0, \text{ otherwise, } j = k \end{cases} \tag{11}$$

with

$$c_{dr} = \frac{D_b}{2} - \sqrt{\frac{D_b^2}{2} - x^2}, c_{di} = r_i - \sqrt{r_i^2 - x^2}, c_{do} = r_o - \sqrt{r_o^2 - x^2}$$

$$r_i = \frac{D_p - D_b}{2}, r_o = \frac{D_p + D_b}{2}$$

$$\Delta\phi_{do} = \frac{2x}{r_o}, \Delta\phi_{di} = \frac{2x}{r_i}$$

where *x* is the half of the spall width. For more details, please refer to [35].

2.2. Deep Residual Network for Fault Detection

Deep residual network (Resnet) is a deep learning method with extremely deep architecture, which shows outstanding performance on accuracy and convergence. It introduces the shortcut connection module into the framework to learn the residual, which avoids the degradation problem of deep networks. The high-level representative features can be better extracted by propagating the data information directly throughout the network [36,37].

A residual learning unit is shown in Figure 4, which can be expressed as:

$$\begin{aligned} \mathbf{y}_l &= h(\mathbf{x}_l) + F(\mathbf{x}_l, \mathbf{W}_l) \\ \mathbf{x}_{l+1} &= f(\mathbf{y}_l) \end{aligned} \tag{12}$$

where $\mathbf{X}_l$ and $\mathbf{X}_{l+1}$ denote the input and output vectors of the *l*th residual unit, which generally includes multi-layers. F is the residual function, which represents the learned residual, while $h(\mathbf{X}_l) = \mathbf{X}_l$ denotes the identity mapping, and $f(\mathbf{y}_l)$ is the activation function. Based on Equation (12), the learning features we obtained from the shallow layer *l* to the deep layer *L* are described as

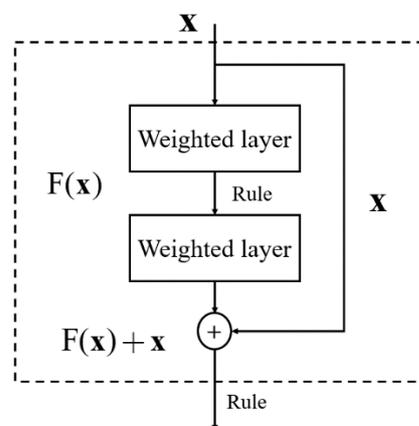$$\mathbf{x}_L = \mathbf{x}_l + \sum_{i=1}^{L-1} F(\mathbf{x}_i, \mathbf{W}_i) \tag{13}$$

Figure 4. A residual learning unit.

With regard to backpropagation, assuming the loss function is E, the gradient of the reverse process can be obtained according to the chain rule of backpropagation.

$$\frac{\partial E}{\partial \mathbf{x}_l} = \frac{\partial E}{\partial \mathbf{x}_L} \cdot \frac{\partial \mathbf{x}_L}{\partial \mathbf{x}_l} = \frac{\partial E}{\partial \mathbf{x}_L} \cdot (1 + \frac{\partial}{\partial \mathbf{x}_l} \sum_{i=1}^{L-1} F(\mathbf{x}_i, \mathbf{W}_i)) \tag{14}$$

where $\frac{\partial E}{\partial \mathbf{x}_L}$ denotes the gradient of the loss function to L, the 1 in parentheses indicates that the shortcut mechanism can propagate the gradient lossless, and the other residual gradient needs to pass through the layer with weight; the gradient is not passed directly. The residual gradient is not all -1 coincidentally, and even if it is small, the presence of 1 will not result in the gradient disappearing. The advantage of the Resnet neural network is that it can be used to train complex networks and ensure high classification accuracy.

3. Experimental Verification

In this section, the open dataset from the Bearing Data Center of Case Western Reserve University is used to verify our method. In order to reduce the process of real data collection, model-based data augmentation is used to construct the training dataset. To reduce the parameters to be identified, Equation (1) can be written as:

$$\begin{aligned} \ddot{y}_s + \frac{c_s}{m_s}\dot{y}_s + \frac{k_s}{m_s}y_s &= \frac{F_r - F_y}{m_s}, \\ \ddot{y}_p + \frac{c_p}{m_p}\dot{y}_p + \frac{k_p}{m_p}y_p &= \frac{F_y}{m_p}. \end{aligned} \tag{15}$$

An error index is used to evaluate the distance between the simulation results and the measured experimental results. To consider the influence of the wave shift, this index is defined in the frequency domain as

$$e_{inx} = \||FFT(\ddot{y}_{p,sim})| - |FFT(\ddot{y}_{p,real})|\| / \||FFT(\ddot{y}_{p,real})|\| \tag{16}$$

where $|FFT(\ )|$ is the amplitude of the frequency.

Then, the system parameters are obtained by solving the optimization problem,

$$\begin{aligned} &\underset{P}{\mathrm{argmin}} e_{inx} \\ &P \in \{c_s/m_s, c_p/m_p, k_s/m_s, k_p/m_p\} \end{aligned} \tag{17}$$

By comparing the simulation data with the experimental data, the parameters of the bearing model can be obtained, as shown in Table 1.

Table 1. Value of parameters in the dynamic equation.

Parameters	Description
c_s/m_s	1000 m/s
c_p/m_p	100 m/s
k_s/m_s	7×10^6 N/m
k_p/m_p	15×10^5 N/m

To better simulate the real situation, a disturbance signal is added in the Equation (1),
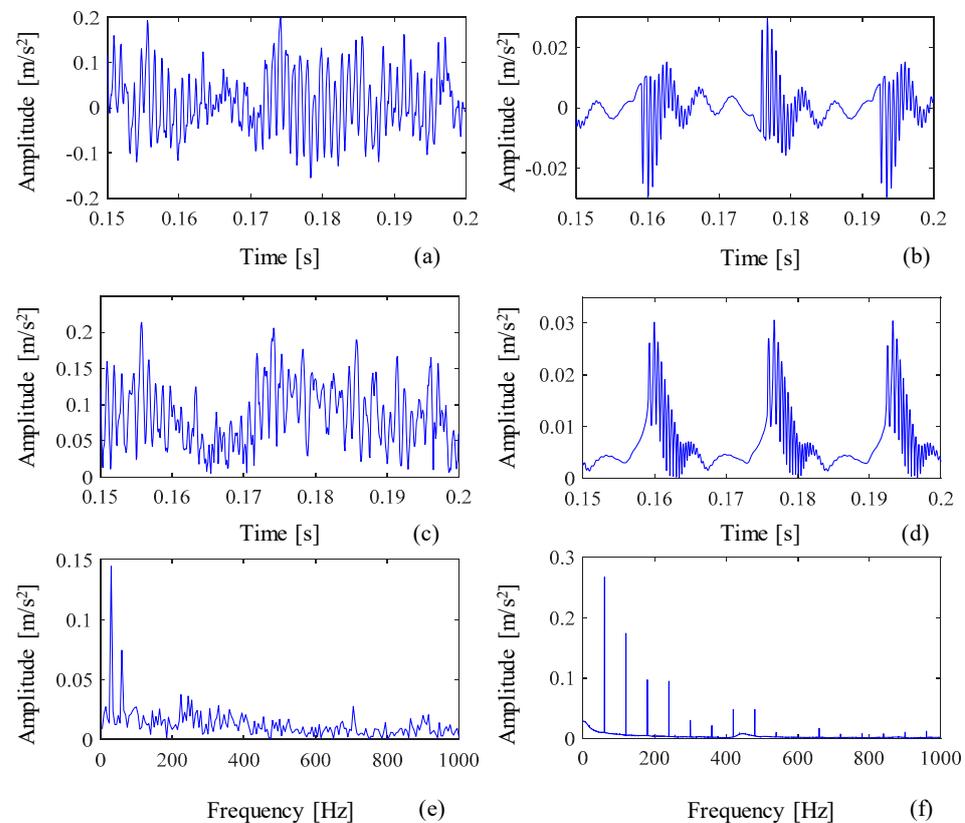
$$m_s\ddot{y}_s + c_s\dot{y}_s + k_sy_s + F_y + F_{ext} = F_r \tag{18}$$
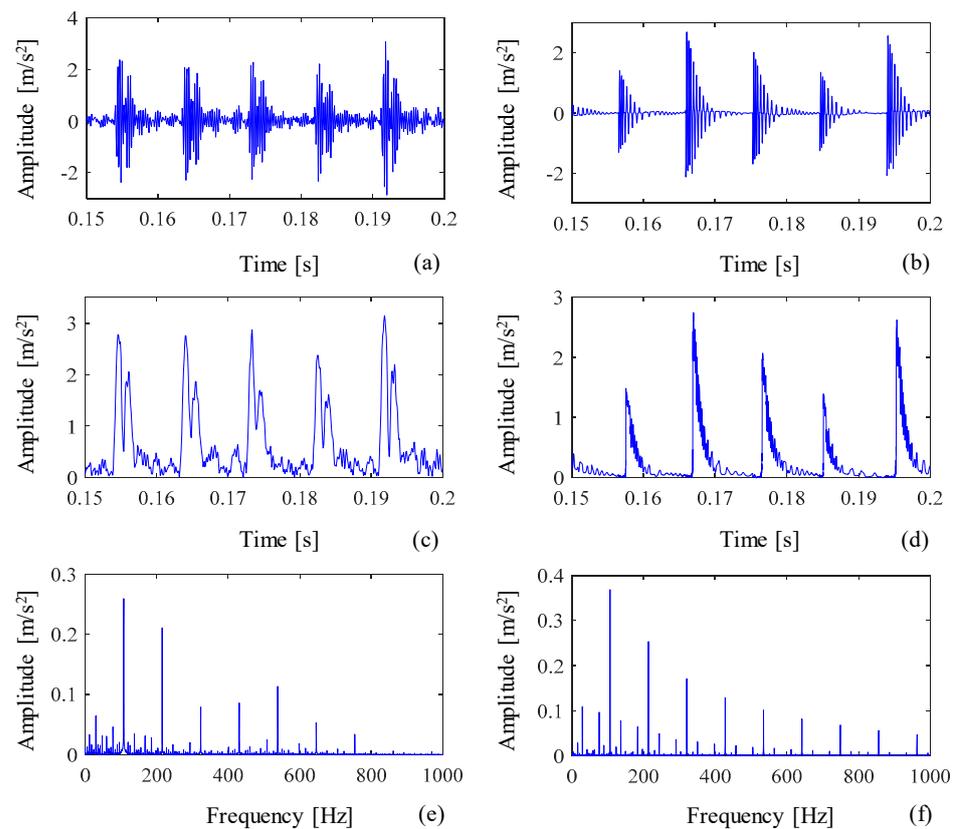
with

$$F_{ext} = A\sin(\omega t)$$

where A is the amplitude of the disturbance force, while ω is the frequency of the disturbance force. In the fault-free case, the information about the disturbance force can be

extracted. Figure 5a shows the experiment in the fault-free case. A vibration with 30 Hz can be measured, which is considered the disturbance force.

Figure 5. Real and simulation data in fault-free cases: (**a**,**c**,**e**) are the original data, the envelop data, and the frequency spectrum of the real envelop data; (**b**,**d**,**f**) are the original data, the envelop data, and the frequency spectrum of the simulation envelop data.

For the purpose of the data augmentation, we used the envelop of the signals instead of the original signals. The reason is that the envelop signals contain less noise. Additionally, the information of the eigenfrequency was not taken into consideration in the envelop signal. Thus, by using envelop signals, we did not need a sufficiently exact model, i.e., the parameter k_s and k_p could deviate to the real value to some extent. Figure 5 gives the real and simulation data in the fault-free case, and (a,c,e) are the original data, the envelop data, and the frequency spectrum of the real envelop data, and (b,d,f) are the original data, the envelop data, and the frequency spectrum of the simulation envelop data, respectively. Figure 6 shows the real and simulation data in the outer race fault case. The task of fault detection is to distinguish the normal case, outer race fault, and inner race fault. Therefore, a Resnet deep neural network was used to design the classifier. The deep neural network shows a powerful ability for classification, but requires mass data for training. Therefore, we used the dynamic model to generate the dataset to assist the training process.

Figure 6. Real and simulation data with outer race fault: (**a**,**c**,**e**) are the original data, the envelop data, and the frequency spectrum of the real envelop data; (**b**,**d**,**f**) are the original data, the envelop data, and the frequency spectrum of the simulation envelop data.

In parameter identification, a group of experiment data is required. After parameter identification, the dynamic model can generate data under different conditions. For example, parameter identification is carried out when the rotation speed is 1797 rpm with a 12 kg load. The model can generate vibration data at different speeds and different loads. Figure 7 shows the generated data with the outer race fault, where (a,c,e) are the original data at different speeds, different pre-loads, and with noise, and (b,d,f) are the envelop data at different speeds, different pre-loads, and with noise. Similarly, the vibration data in the normal case and the inner race fault case can also be generated. Figure 8 shows the simulated vibration data in the inner race fault case. Only a few data are required (such as data with the outer race fault), and the model can generate rich data in different situations.

The Resnet classifier is used for the fault detection of the bearing faults. Table 2 shows the parameters of the Resnet. Three training datasets are constructed for the verification of the proposed method. The first one is the original data. Then, the real envelop dataset and the simulated envelop dataset are used to train the Resnet classifier. The testing dataset includes the normal, outer race fault, and inner race fault cases.
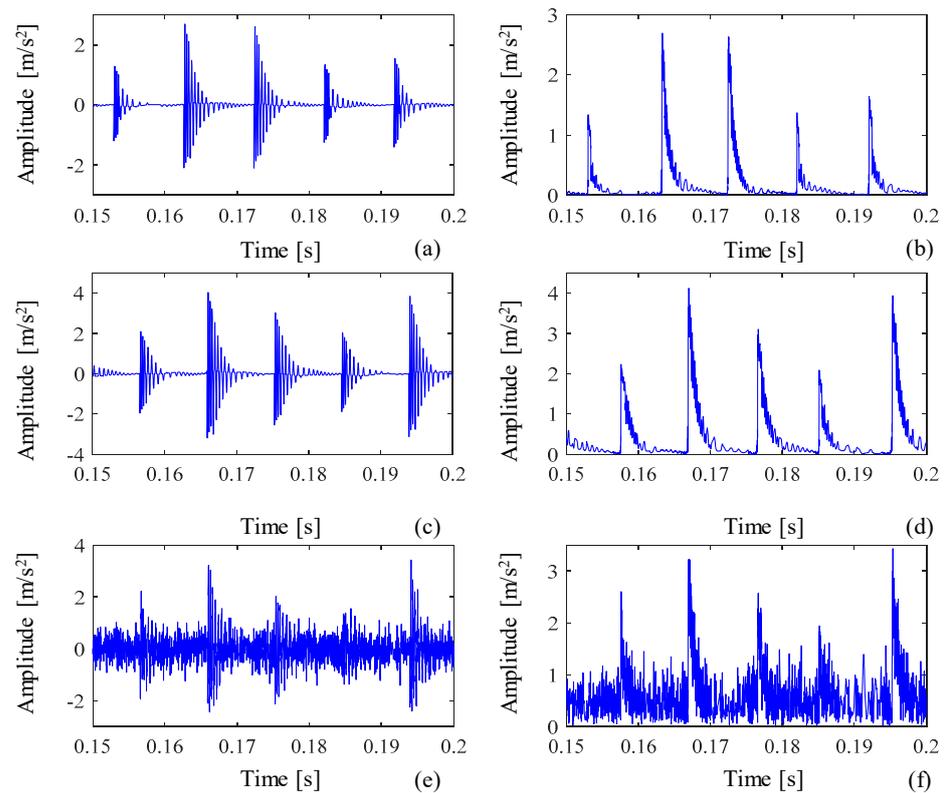
Figure 7. The generated data with the outer race fault: (**a**,**c**,**e**) the original data at different speeds, different pre-loads, and with noise; (**b**,**d**,**f**) are the envelop data at different speeds, different pre-loads, and with noise.
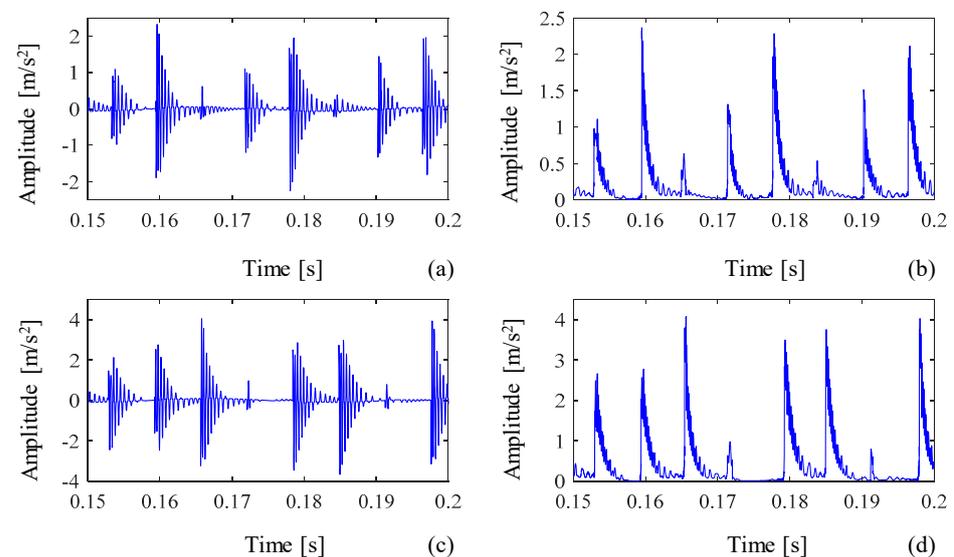

Figure 8. The generated data with inner race fault: (**a**,**b**) are the original data and the envelop data when the rotation speed is 1797 rpm; (**c**,**d**) are the original data and the envelop data when the rotation speed is 1730 rpm.

Table 2. Structure parameters of Resnet.

| Description		Value	
The resolution of input signals		1×2000	
	Layer name	Output size	Layer
	Conv1	1×1000	$3 \times 3, 8$
	Conv2	1×500	$\begin{bmatrix} 3 \times 3, & 16 \\ 3 \times 3, & 16 \end{bmatrix} \times 3$
	Conv3	1×250	$\begin{bmatrix} 3 \times 3, & 32 \\ 3 \times 3, & 32 \end{bmatrix} \times 4$
The size of the network	Conv4	1×125	$\begin{bmatrix} 3 \times 3, & 64 \\ 3 \times 3, & 64 \end{bmatrix} \times 6$
	Conv5	1×64	$\begin{bmatrix} 3 \times 3, & 128 \\ 3 \times 3, & 128 \end{bmatrix} \times 3$
	GAP	1×2	128
Activation function		Sigmoid	

In general, if smaller differences exist between the simulation data and the real data, the classified results will be more accurate. However, the gap between the simulation and the real data will always exist. This is the reason why we use the envelop data instead of the original data. Figure 9 shows the comparison results between the simulation and real data. The error index is used to evaluate the performance of the simulation results for data augmentation. The error index for the original data is 0.9214, while the error index for the envelop data is 0.4622. The gap between the real and simulation results of the original data is much larger than that of the envelop data. This is the reason why we use the envelop data as the training dataset. training cost, which has a large application prospect.
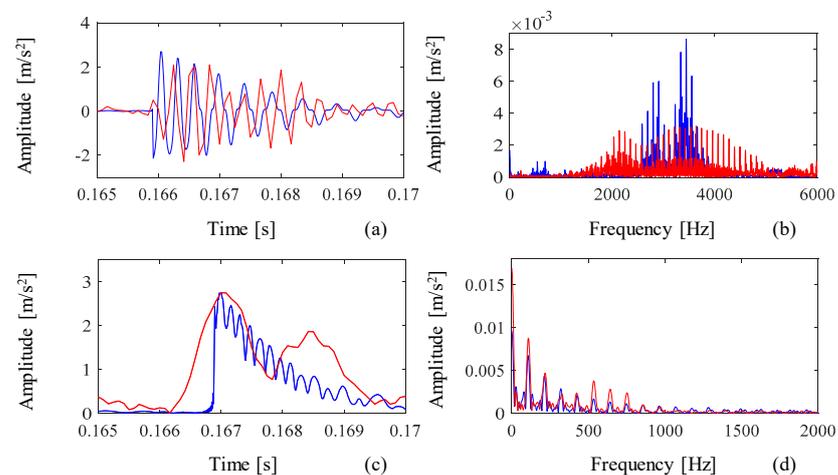
Figure 9. Comparison of experimental and simulation data: (**a**,**c**) are the data in the time domain; (**b**,**d**) are the data in the frequency domain, where the blue line is the experiment data, and the red line is the simulation data.

Figure 10 shows the distribution of the probability of each dataset after training. The training dataset contains 500 groups of data, while the testing dataset contains 150 groups of data. If the real data (the original data and the envelop data) are used for training, the classified accuracy can reach 100%. The reason for this is that the difference is great for the signal in the three cases. However, the collection of the data in different operation situations is expensive work. Figure 10c shows the classification results of the Resnet classifier, which is trained by pure simulation data. The classified accuracy is still 100%, but the possibility is lower than that by using the real data. The reason for this is that the simulation data

is not the same as the real data. A gap between the simulation and real data therefore results in a low possibility. By using the envelop data, we can reduce the gap and achieve accepted classification results. The proposed method, based on the Resnet classifier with model-based data augmentation, can overcome the high costs of the classifier training cost, which has a large application prospect.
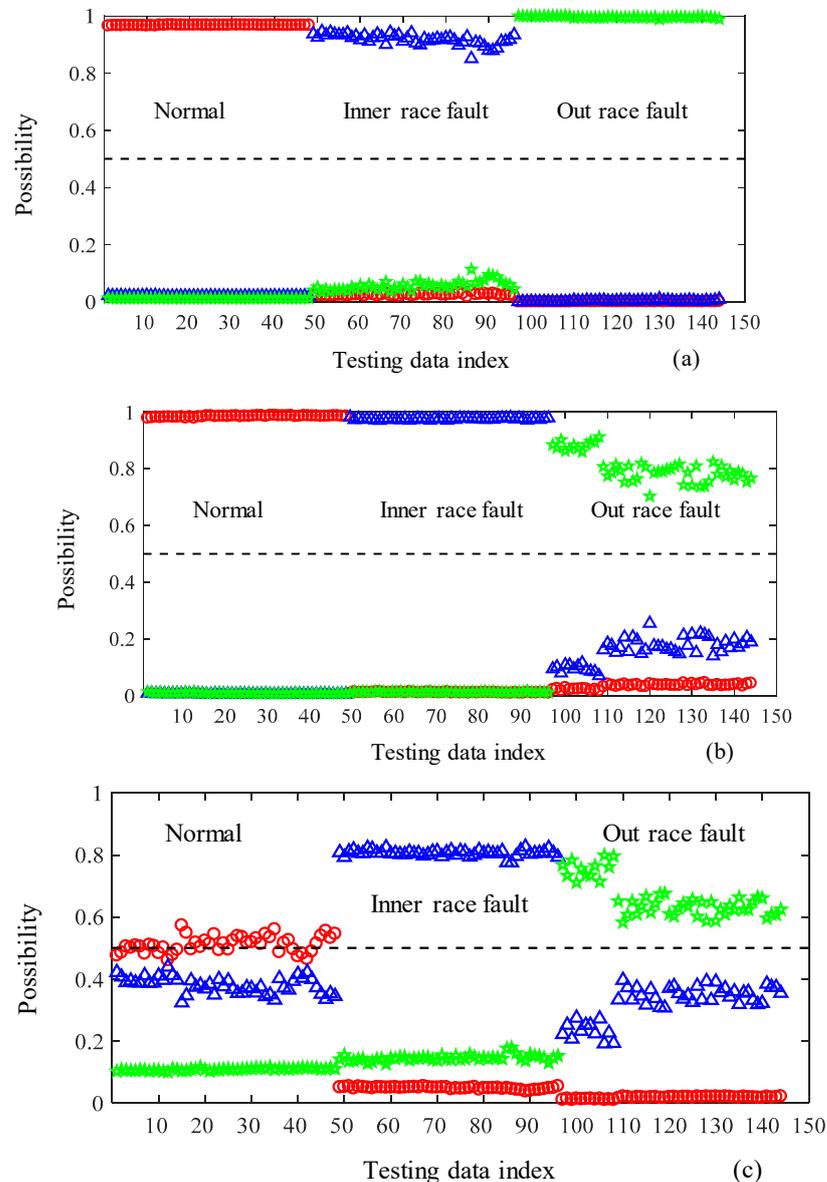
Figure 10. Classification results of the Resnet classifier: (**a**) the training and testing datasets are the real original data; (**b**) the training and testing datasets are the real envelop data; (**c**) the training dataset is the simulation data while the testing dataset is the real data.

4. Conclusions

In this paper, a bearing fault detection method, based on a Resnet classifier with model-based data augmentation, is proposed. For our purpose, a four-DOFs dynamic model is constructed to describe the bearing system. The dynamic model was identified by comparing the simulation and experimental results. Then, a large number of data under different conditions could then be generated, based on which the training dataset was constructed, and the Resnet classifier was trained for the bearing state classification. Furthermore, to reduce the gap between the simulation data and the real data, the envelop signals were applied in the training process rather than the original signals. The proposed

method was testified by the real data from the Bearing Data Center of Case Western Reserve University. The trained Resnet classifier was able to identify the bearing states with 100% accuracy. The framework of the proposed method, based on data augmentation, which combines the theoretical model with the deep learning method, can be further used in other fields which have the deterministic model.

Author Contributions: For research articles with several authors, Conceptualization, L.Q. and X.Z.; methodology, L.Q. and Q.P.; software, Y.L.; validation, L.Q., Y.L. and X.Z.; formal analysis, Q.P.; investigation, L.Q.; resources, Y.L.; data curation, L.Q.; writing—original draft preparation, L.Q.; writing—review and editing, Y.L.; visualization, Q.P.; supervision, Y.L.; project administration, X.Z.; funding acquisition, X.Z. All authors have read and agreed to the published version of the manuscript.

Informed Consent Statement: Not applicable.

Data Availability Statement: Not applicable.

Conflicts of Interest: The authors declare no conflict of interest.

Nomenclature

x_s, y_s	shaft/inner race DOF
x_p, y_p	pedestal/outer race DOF
m_s	mass of shaft/inner race
m_p	mass of pedestal/outer race
c_s	damping of shaft/inner race
c_p	damping of pedestal/outer race
k_s	stiffness of shaft/inner race
D_b	ball diameter
D_P	pitch circle diameter
ω_s	angular velocity of the shaft
ω_c	angular velocity of the cage
ω_r	angular velocity of the rolling element
ϕ_j	angular position of the rolling elements
δ	overall contact deformation
c	clearance value
ϕ_0	initial angular position of cage
c_d	fault depth
ϕ_d	angular position of the fault
ϕ_{d0}	initial angular position of the fault

References

1. Qian, L. *Observer-Based Fault Detection and Estimation of Rolling Element Bearing Systems*; Shaker Verlag: Herzogenrath, Germany, 2019.
2. Gao, Z.; Cecati, C.; Ding, S.X. A survey of fault diagnosis and fault-tolerant techniques—Part I: Fault diagnosis with model-based and signal-based approaches. *IEEE Trans. Ind. Electron.* **2015**, *62*, 3757–3767. [CrossRef]
3. Mebarki, N.; Benmoussa, S.; Djeziri, M.; Mouss, L.H. New Approach for Failure Prognosis Using a Bond Graph, Gaussian Mixture Model and Similarity Techniques. *Processes* **2022**, *10*, 435. [CrossRef]
4. Zhang, Z.; Si, X.; Hu, C.; Lei, Y. Degradation data analysis and remaining useful life estimation: A review on Wiener-process-based methods. *Eur. J. Oper. Res.* **2018**, *271*, 775–796. [CrossRef]
5. Lv, Y.; Zhao, W.; Zhao, Z.; Li, W.; Ng, K.K. Vibration signal-based early fault prognosis: Status quo and applications. *Adv. Eng. Inform.* **2022**, *52*, 101609. [CrossRef]
6. Pająk, M.; Muślewski, Ł.; Landowski, B.; Kałaczyński, T.; Kluczyk, M.; Kolar, D. Identification of Reliability States of a Ship Engine of the Type Sulzer 6AL20/24. *SAE Int. J. Engines* **2021**, *15*, 527–542. [CrossRef]
7. Dyer, D.; Stewart, R. Detection of rolling element bearing damage by statistical vibration analysis. *J. Mech. Des.* **1978**, *100*, 229–235. [CrossRef]

8. Choy, K.; Gunter, E.; Allaire, P. Fast fourier transform analysis of rotor-bearing systems. Topics in Fluid Film Bearing and Rotor Bearing System Design and Optimization. 1978. Available online: https://www.academia.edu/download/86674071/fast_fourier_transform_analysis_of_rotot1980v2_linked.pdf (accessed on 27 May 2022).

9. Too, J.; Abdullah, A.R.; Mohd Saad, N.; Mohd Ali, N. Feature selection based on binary tree growth algorithm for the classification of myoelectric signals. *Machines* **2018**, *6*, 65. [CrossRef]

10. Zhou, Y.; Wang, J.; Wang, Z. Bearing Faulty Prediction Method Based on Federated Transfer Learning and Knowledge Distillation. *Machines* **2022**, *10*, 376. [CrossRef]

11. Sun, Q.; Tang, Y. Singularity analysis using continuous wavelet transform for bearing fault diagnosis. *Mech. Syst. Signal Process.* **2002**, *16*, 1025–1041. [CrossRef]

12. Lei, Y.; Lin, J.; He, Z.; Zuo, M.J. A review on empirical mode decomposition in fault diagnosis of rotating machinery. *Mech. Syst. Signal Process.* **2013**, *351*, 108–126. [CrossRef]

13. Chen, H.; Chai, Z.; Dogru, O.; Jiang, B.; Huang, B. Data-driven designs of fault detection systems via neural network-aided learning. *IEEE Trans. Neural Netw. Learn. Syst.* **2021**, 1–12. [CrossRef]

14. Yuan, H.; Wu, N.; Chen, X.; Wang, Y. Fault diagnosis of rolling bearing based on shift invariant sparse feature and optimized support vector machine. *Machines* **2021**, *9*, 98. [CrossRef]

15. Yiakopoulos, C.T.; Gryllias, K.C.; Antoniadis, I.A. Rolling element bearing fault detection in industrial environments based on a K-means clustering approach. *Expert Syst. Appl.* **2011**, *38*, 2888–2911. [CrossRef]

16. Samanta, B.; Al-Balushi, K.; Al-Araimi, S. Artificial neural networks and support vector machines with genetic algorithm for bearing fault detection. *Eng. Appl. Artificial Intell.* **2003**, *16*, 657–665. [CrossRef]

17. Lv, Y.; Zhou, Q.; Li, Y.; Li, W. A predictive maintenance system for multi-granularity faults based on AdaBelief-BP neural network and fuzzy decision making. *Adv. Eng. Inform.* **2021**, *49*, 101318. [CrossRef]

18. Shi, Q.; Zhang, H. Fault diagnosis of an autonomous vehicle with an improved SVM algorithm subject to unbalanced datasets. *IEEE Trans. Ind. Electron.* **2020**, *68*, 6248–6256. [CrossRef]

19. Zhang, N.; Li, Y.; Yang, X.; Zhang, J. Bearing Fault Diagnosis Based on BP Neural Network and Transfer Learning. *J. Phys. Conf. Ser.* **2021**, *1881*, 022084. [CrossRef]

20. Ding, H.; Gao, R.X.; Isaksson, A.J.; Landers, R.G.; Parisini, T.; Yuan, Y. State of AI-based monitoring in smart manufacturing and introduction to focused section. *IEEE/ASME Trans. Mechatron.* **2020**, *25*, 2143–2154. [CrossRef]

21. Lei, Y.; Jia, F.; Lin, J.; Xing, S.; Ding, S.X. An intelligent fault diagnosis method using unsupervised feature learning towards mechanical big data. *IEEE Trans. Ind. Electron.* **2016**, *63*, 3137–3147. [CrossRef]

22. Kolar, D.; Lisjak, D.; Pająk, M.; Pavković, D. Fault diagnosis of rotary machines using deep convolutional neural network with wide three axis vibration signal input. *Sensors* **2020**, *20*, 4017. [CrossRef]

23. Janssens, O.; Slavkovikj, V.; Vervisch, B.; Stockman, K.; Loccufier, M.; Verstockt, S.; Van de Walle, R.; Van Hoecke, S. Convolutional neural network based fault detection for rotating machinery. *J. Sound Vib.* **2016**, *377*, 331–345. [CrossRef]

24. Mao, W.; Feng, W.; Liang, X. A novel deep output kernel learning method for bearing fault structural diagnosis. *Mech. Syst. Signal Process.* **2019**, *117*, 293–318. [CrossRef]

25. Zhang, R.; Tao, H.; Wu, L.; Guan, Y. Transfer learning with neural networks for bearing fault diagnosis in changing working conditions. *IEEE Access* **2017**, *5*, 14347–14357. [CrossRef]

26. LeCun, Y.; Bottou, L.; Bengio, Y.; Haffner, P. Gradient-based learning applied to document recognition. *Proc. IEEE* **1998**, *86*, 2278–2324. [CrossRef]

27. Shijie, J.; Ping, W.; Peiyi, J.; Siping, H. Research on data augmentation for image classification based on convolution neural networks. In Proceedings of the 2017 Chinese Automation Congress CAC, Jinan, China, 2–22 October 2017; IEEE: Piscataway, NJ, USA; p. 4165.

28. Kim, S.; Kim, N.H.; Choi, J.H. Prediction of remaining useful life by data augmentation technique based on dynamic time warping. *Mech. Syst. Signal Process.* **2020**, *136*, 106486. [CrossRef]

29. Yu, K.; Lin, T.R.; Ma, H.; Li, X. A multi-stage semi-supervised learning approach for intelligent fault diagnosis of rolling bearing using data augmentation and metric learning. *Mech. Syst. Signal Process.* **2021**, *146*, 107043. [CrossRef]

30. Hu, T.; Tang, T.; Chen, M. Data simulation by resampling—A practical data augmentation algorithm for periodical signal analysis-based fault diagnosis. *IEEE Access* **2019**, *7*, 125133–125145. [CrossRef]

31. Lu, H.; Zhao, X.; Tao, B.; Ding, H. A state-classification approach for light-weight robotic drilling using model-based data augmentation and multi-level deep learning. *Mech. Syst. Signal Process.* **2022**, *167*, 108480. [CrossRef]

32. Sobie, C.; Freitas, C.; Nicolai, M. Simulation-driven machine learning: Bearing fault classification. *Mech. Syst. Signal Process.* **2018**, *99*, 403–419. [CrossRef]

33. Chen, H.; Jiang, B.; Ding, S.X.; Huang, B. Data-driven fault diagnosis for traction systems in high-speed trains: A survey, challenges, and perspectives. *IEEE Trans. Intell. Transp. Syst.* **2020**, *23*, 1700–1716. [CrossRef]

34. Chen, H.; Jiang, B. A review of fault detection and diagnosis for the traction system in high-speed trains. *IEEE Trans. Intell. Transp. Syst.* **2019**, *21*, 450–465. [CrossRef]

35. Sawalhi, N.; Randall, R.B. Simulating gear and bearing interactions in the presence of faults: Part I. The combined gear bearing dynamic model and the simulation of localised bearing faults. *Mech. Syst. Signal Process.* **2008**, *22*, 1924–1951. [CrossRef]

36. He, K.; Zhang, X.; Ren, S.; Sun, J. Deep residual learning for image recognition. In Proceedings of the IEEE Conference on Computer Vision and Pattern Recognition, Las Vegas, NV, USA, 27–30 June 2016; pp. 770–778.

37. Zhang, W.; Li, X.; Ding, Q. Deep residual learning-based fault diagnosis method for rotating machinery. *ISA Trans.* **2019**, *95*, 295–305. [CrossRef] [PubMed]